DRAFT VERSION JANUARY 28, 2020
Typeset using LaTeX **twocolumn** style in AASTeX62

WASP-4 is Accelerating Towards the Earth

L. G. BOUMA,[1] J. N. WINN,[1] A. W. HOWARD,[2] S. B. HOWELL,[3] H. ISAACSON,[4] H. KNUTSON,[5] AND R. A. MATSON[3]

[1] *Department of Astrophysical Sciences, Princeton University, 4 Ivy Lane, Princeton, NJ 08540, USA*
[2] *Cahill Center for Astrophysics, California Institute of Technology, Pasadena, CA 91125, USA*
[3] *NASA Ames Research Center, Moffett Field, CA 94035, USA*
[4] *Astronomy Department, University of California, Berkeley, CA 94720, USA*
[5] *Division of Geological and Planetary Sciences, California Institute of Technology, Pasadena, CA 91125, USA*

(Received January 28, 2020; Revised —; Accepted —)

Submitted to AAS journals.

ABSTRACT

Space and ground-based transit observations of the hot Jupiter WASP-4b have recently indicated that its orbital period is decreasing. The period change could be caused by tidal orbital decay, orbital precession, or light-travel time effects. In this work we present new radial velocity measurements of WASP-4, acquired with Keck-HIRES. The data show that the system is accelerating towards the Earth at $\dot{\gamma} = -0.0422^{+0.0028}_{-0.0027}$ m s^{-1} yr^{-1}. This implied period decrease probably explains WASP-4's changing orbital period as a light-travel time effect. By combining the radial velocities with new limits from speckle imaging, we find that system's acceleration is likely caused by a 10-200 $M_{\rm Jup}$ companion with semi-major axis between 10-100 AU. Based on statistics from Knutson et al. (2014), about 1 in 6 hot Jupiters are expected to show period decreases commensurate with WASP-4 due to acceleration by outer companions. These period decreases will be increasingly measureable in coming years, because the precision of period derivative measurements scales as the fourth power of the observing baseline. Continued long-term radial velocity monitoring of hot Jupiters is therefore essential to distinguish tidal orbital decay from line-of-sight accelerations.

Keywords: Exoplanet tides (497), Exoplanet dynamics (490), Radial velocity (1332), Transit timing variation method (1710)

1. INTRODUCTION

The issue of whether and how the orbits of hot Jupiters decay due to tidal interaction with their host stars has drawn significant attention over the past 25 years (Rasio et al. 1996; Levrard et al. 2009; Matsumura et al. 2010). Numerous observations have also been performed (CITE). These efforts are now yielding fruit: by combining transit and occultation timing with radial velocity measurements, Yee et al. (2020) have shown that the data for the hot Jupiter WASP-12b are most compatible with orbital decay.

The present study highlights a point that, though obvious, has perhaps not yet received due attention. The point is that observational programs aimed at identifying orbital decay in hot Jupiters will be crippled without long-term radial velocity monitoring programs. The reason is simple: when the timescale of orbital period change exceeds the observing baseline, the first deviation from constant periodicity is always quadratic in the transit number.

While orbital decay may be common (CITE). line-of-sight accelerations could be even *more* common (CITE Knutson 14, Bryan 16). Both manifest to first order identically in transit times (up to the sign of the line-of-sight acceleration) – as a non-zero period derivative. Specifically, Knutson et al. (2014) showed that X% of hot Jupiters show some form of radial acceleration in radial velocity time-series with baselines of YY years. Assuming a separation distribution of (WHATEVER), this implies that ZZ% of hot Jupiters will *always* show a changing orbital period, over timescale of say 10 years.

The main focus of this study is the hot Jupiter WASP-4b, which has an orbital period that appears to be decreasing by about 10 milliseconds per year. We discovered the timing variations using data from TESS and a decade of ground-based observations (Bouma et al. 2019, hereafter B19). Thereafter, Southworth et al. (2019) reported 22 new transit times for the system, and found an updated decay rate of $\dot{P} = -9.2 \pm 1.1$ milliseconds per year. The Southworth et al. decay rate was $\approx 3\sigma$ less rapid than that found

Corresponding author: L. G. Bouma
luke@astro.princeton.edu

by B19, but the conclusions of the studies were otherwise the same. A separate study by Baluev et al. (2019) reported additional archival transit light curves of WASP-4b, most notably from the TRAPPIST archive, as well as from select other observers. Baluev et al. (2019) pointed out that when using lower-precision subsets of the available transit data, the case for a decreasing period worsened. We agree with this statement.

To determine the origin of the period change, we acquired four additional radial velocity measurements using Keck-HIRES, extending the RV baseline from 3 to 9 years. Previously, the five available HIRES radial velocities suggested a weak ($< 2\sigma$) linear trend (Knutson et al. 2014). Our new measurements reveal a line-of-sight acceleration of $\dot{\gamma} = -0.0422^{+0.0028}_{-0.0027}$ m s^{-1} yr^{-1}. This translates to an expected period decrease from the light-travel time effect of -5.9 milliseconds per year—about commensurate with what is observed from transits. In the following, we avoid the term "Rømer delay", which typically signifies arrival time delay due to observatory motion. We are discussing the Doppler effect seen by a stationary observer for a source with constant line-of-sight acceleration.

In the following, § 2 collects the available transit data and presents the new radial velocity and speckle imaging observations. § 3 analyzes the data, and finds that they yield a picture in which the WASP-4 system is accelerating towards our line-of-sight, likely due to the pull of a brown or M-dwarf companion. § 4 places this result in the broader context of orbital decay searches, and points out that line-of-sight accelerations, *i.e.*, "false positive orbital decay signals", are relatively common for the hot Jupiter population. § 5 offers brief concluding remarks.

2. OBSERVATIONS

2.1. *Transits*

Table N lists the transit times we collected for our analysis. We include data from the peer-reviewed literature for which (a) the analysis was based on observations of a single transit, (b) the midpoint was fitted as a free parameter, and (c) the time system specified both the leap second correction (TDB or UTC) and also whether any barycentric or heliocentric corrections had been performed.

The majority of times are identical to those we collected in B19. Twenty-two new times reported by Southworth et al. (2019) are included. These transits were observed from the 3.58m NTT and Danish 1.54m telescopes at La Silla, and the SAAO 1.0m telescope.

Additional timimg measurements have also recently been reported by Baluev et al. (2019), based on a homogeneous analysis of archival ground-based observations taken professional and amateur observers. We included twelve of their "high quality" transit times acquired by TRAPPIST (six transits), El Sauce (four transits), and Petrucci et al. (2013). For TRAPPIST and El Sauce, we verified with the original observers that correct barycentric and leap-second corrections had been performed (M. Gillon, P. Evans, priv. comm.). We omitted the fourteen remaining Baluev et al. ETD[1] times due to ambiguity in whether leap-second corrections had or had not been performed.

The four available occultations tabulated by B19 have negligible statistical value due to their large uncertainties, and we forgo their use in this analysis.

2.2. *Radial velocities*

After identifying the period decrease in B19, we acquired four additional radial velocity measurements with the Keck High Resolution Echelle Spectrometer (HIRES, Vogt et al. 1994). Our observations were acquired under the purview of the California Planet Survey (Howard et al. 2010). The spectra were reduced using **software X**. Previously, the HIRES data-points spanned 2010 to 2013 (Knutson et al. 2014). Our new measurements triple the HIRES observing baseline to nine years.

The complete set of radial velocity observations is given in **Table M**. Along with the 2010-2019 HIRES observations, there are also earlier measurements from CORALIE and HARPS. Following B19, we included the CORALIE measurements from Wilson et al. (2008) and Triaud et al. (2010), using the homogeneous radial velocities calculated by the latter authors. We included the HARPS values reported by Pont et al. (2011) and Husnoo et al. (2012). We omitted the HARPS data points taken over three nights by Triaud et al. (2010) for Rossiter-McLaughlin observations because they have a systematic offset from the remaining datasets.

2.3. *Speckle imaging*

A cursory analysis of the new HIRES observations led to our detection of a linear trend in the residuals after fitting out the orbit of WASP-4b. This prompted us to acquire speckle images using Zorro at Gemini-South (see Scott et al. 2018, and the instrument web-pages[2]). Zorro is a dual-channel speckle interferometer with narrow-band filters centered at 562 nm and 832 nm.

We observed WASP-4 twice, on the night of September 11-12 (8 sets of 1000 frames each) and also on the night of September 28-29 (7 sets of 1000 frames each). **We reconstructed the images following... We reduced the reconstructed speckle images to contrast curves by injecting and recovering point-sources...** The contrast curves showed that the second night, which had better seeing, also produces the more constraining result. The 832 nm results were also typically the most constraining, since faint companions are typically redder. We therefore opt for the 832 nm September 28-29 results for the remaining analysis.

3. ANALYSIS

3.1. *Transits*

We considered two models for the observed transit times. The first model assumes a constant orbital period on a circu-

[1] http://var2.astro.cz/ETD

[2] www.gemini.edu/sciops/instruments/alopeke-zorro/

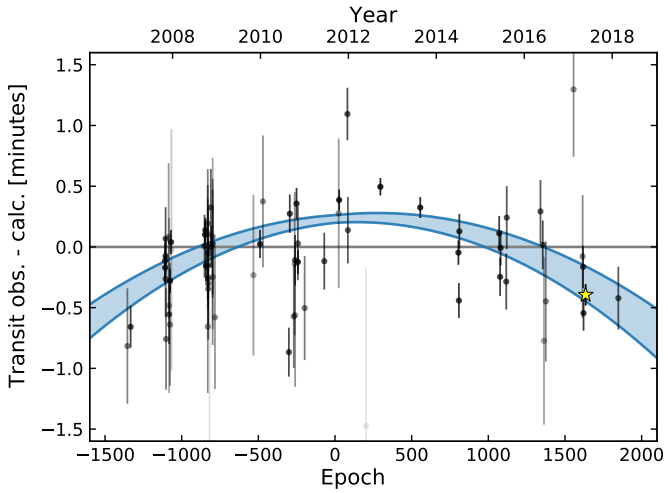

Figure 1. Timing residuals and best-fit models for WASP-4b. The vertical axis shows the observed transit times minus the calculated times assuming a constant orbital period. More opaque points correspond to more precise data. The quadratic ephemeris and its $\pm 1\sigma$ statistical uncertainties are shown in blue. Neither model fully explains the scatter in transit residuals, perhaps due to underestimated uncertainties (see 3.1). The binned TESS point (yellow star) is the weighted average of 18 TESS transits and is binned for display purposes only. Its uncertainty is slightly larger than the marker size. The models were fitted to all of the individual transit times.

lar orbit:

$$t_{\rm tra}(E) = t_0 + PE, \tag{1}$$

where E is the epoch number and t_0 is a reference epoch. The second model assumes that the period changes at a steady rate:

$$t_{\rm tra}(E) = t_0 + PE + \frac{1}{2}\frac{{\rm d}P}{{\rm d}E}E^2. \tag{2}$$

The free parameters are the reference epoch t_0, the period at the reference epoch P, and the period derivative, ${\rm d}P/{\rm d}t = (1/P){\rm d}P/{\rm d}E$. We defined the epoch numbers such that $E = 0$ is near the weighted average of the observed times. This helps to reduce the covariance between t_0 and P. A third possible model that we did not consider for reasons that will become apparent is a precessing, eccentric orbit (*e.g.*, Giménez & Bastero 1995; Patra et al. 2017).

We fitted each of the two models by assuming a Gaussian likelihood and sampling over the posterior probability distributions. We sampled the posterior using the algorithm proposed by Goodman & Weare (2010) and implemented by Foreman-Mackey et al. (2013) in `emcee`. The prior for the quadratic model allowed the period derivative to have any sign.

Figure 1 shows the observed transit times, minus the best-fit constant period model. The best-fitting constant-period model has $\chi^2 = 276$, 91 degrees of freedom, and $\chi^2_{\rm red} = 3.0$. The best-fitting quadratic model has $\chi^2 = 183$, 90 degrees of freedom, and $\chi^2_{\rm red} = 2.0$. The difference in the Bayesian information criteria (BIC) between the linear and quadratic and models is $\Delta{\rm BIC} = 89.1$, strongly favoring the quadratic case (Kass & Raftery 1995).

From the reduced χ^2 values, we can surmise that neither model entirely describes the transit data that we have collected—there must be some additional source of signal or noise. In Bouma et al. (2019), we found that the quadratic model for the (sparser) transit data gave $\chi^2_{\rm red} = 1.0$. The worsened $\chi^2_{\rm red}$ could reflect underestimated statistical uncertainties in any of our transit measurements. It could also reflect systematic errors in the time-systems in which the transit measurements were recorded, though we have taken every caution against this latter possibility.

One approach to analyzing such data would be to introduce a fudge factor that inflates the transit measurement uncertainties, and lowers the reduced χ^2. We do not think that such an approach is warranted, since it would not change the result that the quadratic model is strongly preferred.

The best-fit period derivative in the quadratic model is

$$\dot{P} = -(2.74 \pm 0.28) \times 10^{-10} = -8.64 \pm 0.89 \ {\rm ms\,yr^{-1}}. \tag{3}$$

This agrees to within 1σ of the value reported by Southworth et al. (2019) ($\dot{P} = -9.2 \pm 1.1$ ms yr^{-1}). It is $\approx 3\sigma$ larger than the rate of period decrease we found earlier (-12.6 ± 1.2 ms yr^{-1}; Bouma et al. 2019), presumably because of missing coverage filled in by Southworth et al.'s and Baluev et al.'s observations. The other best-fit transit timing model parameters are reported in **Table X**.

3.2. *Radial Velocities: WASP-4's acceleration towards the Earth*

Our initial model for the radial velocity data was a single Keplerian orbit, plus instrument offsets, jitters, and a long-term trend (Fulton et al. 2018, `radvel`). We set Gaussian priors on the orbital period and time of inferior conjunction using the values from Table 4 of B19, and fixed WASP-4b's eccentricity to zero (Beerer et al. 2011; Knutson et al. 2014; Bonomo et al. 2017). The free parameters were the velocity semi-amplitude, the instrument zero-points, an additive "white noise" instrument jitter for each instrument, linear ($\dot{v}_{\rm r}$), and optionally second-order ($\ddot{v}_{\rm r}$) acceleration terms.

We found that the best-fitting model with both linear and quadratic radial velocity terms was marginally preferred (by $\Delta{\rm BIC} = 5.8$) over the best-fitting model with only a linear term. Regardless, for consistency with Knutson et al. (2014), who fixed the quadratic component of the long-term trend to zero, in Figure 2 we show best-fitting models for the linear-trend case.

WASP-4 was found to be accelerating towards our line-of-sight at high confidence,

$$\dot{v}_{\rm r} = \dot{\gamma} = -0.0422^{+0.0028}_{-0.0027} \ {\rm m\,s^{-1}\,day^{-1}}. \tag{4}$$

For comparison, before our new measurements, $\dot{v}_{\rm r}$ was thought to be about five times smaller, and was only

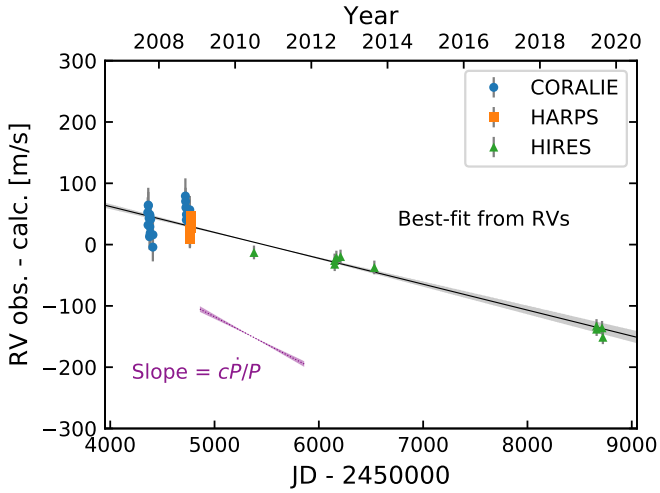

Figure 2. Radial velocity observations of WASP-4. The best-fit Keplerian orbit of WASP-4b has been subtracted. The linear trend inferred from the RV data is shown with a black line, with 1σ errors in gray. The trend that would be needed to produce the period decrease seen in transits ($\dot{P} = -8.64 \pm 0.89$ ms yr^{-1}) is indicated with the purple dotted line. The four new RV measurements presented in this work increased the significance of the radial velocity trend from $\approx 2\sigma$ to 15σ.

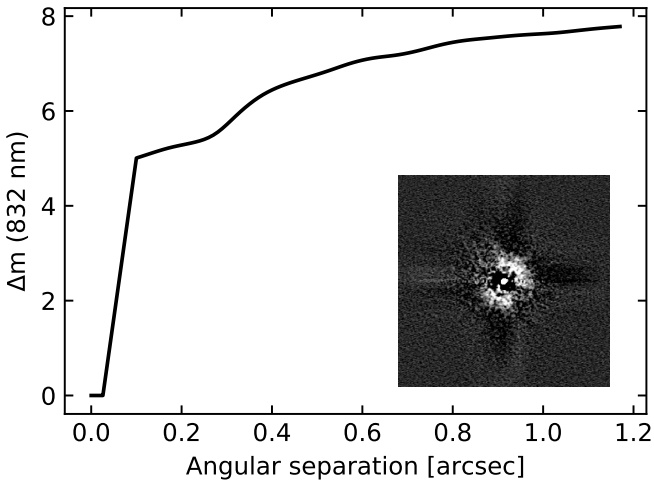

Figure 3. Zorro contrast curve derived from point-source injection-recovery experiments. Sources below the curve would have been detected. The inset shows the speckle image reconstructed from 1000 40 millisecond frames in an 832 nm bandpass, and acquired on September 28, 2019. The image scale is $2.46'' \times 2.46''$.

marginally significant (Knutson et al. 2014; Bouma et al. 2019).

The system's acceleration towards our line-of-sight causes a decrease in the apparent orbital period. The period derivative expected from radial velocities is

$$\dot{P}_{\rm RV} = \frac{\dot{v}_{\rm r} P}{c} = -5.94 \pm 0.39 \text{ ms yr}^{-1}. \quad (5)$$

In other words, the majority of the period decrease observed in transits ($\dot{P} = -8.64 \pm 0.89$ ms yr^{-1}) seems to be explained by the acceleration of the host star.

An important consideration is whether the measured RV trend is correlated with stellar activity. We investigate this by analyzing WASP-4's emission in the Ca II H & K lines, as quantified with the chromospheric S-index (Wright et al. 2004). We only examined the HIRES velocities for this step, since they are the main source of signal for our analysis. First, we subtracted the orbital solution from the Keck-HIRES velocities. Then, following Bryan et al. (2016, 2019), we calculated the Spearman rank correlation coefficient between the S-index and the orbit-subtracted velocities. We found a correlation coefficient of 0.16. This correlation is not statistically significant; the corresponding p-value is 0.65. Furthermore, inspection of the S-index timeseries showed no secular or sinusoidal trends, as would be expected if we were observing a long-term magnetic activity cycle. The S-index values are included in **Table X**. We conclude that it is highly unlikely that the linear trend is caused by stellar activity.

3.3. *Constraints on companion masses and semi-major axes*

Given a linear radial velocity trend, we can place lower-limits on the mass and semi-major axis of additional bodies in the system. As a quick estimate of the minimum mass required to explain the linear trend in WASP-4, we turn to Feng et al. (2015). As they discuss, the scenario that yields the minimum companion mass for a system with a linear trend is a companion with $e \approx 0.5$ and $\omega = 90°$. From their Equation 1,

$$M_{\rm min} \approx 0.0164 M_{\rm Jup} \left(\frac{\tau}{\rm yr}\right)^{4/3} \left|\frac{\dot{\gamma}}{\rm m\,s^{-1}\,yr^{-1}}\right| \left(\frac{M_\star}{M_\odot}\right)^{2/3}, \quad (6)$$

where τ is the observing baseline. For WASP-4, this yields $M_{\rm min} = 4.7 M_{\rm Jup}$. Higher mass companions are allowed, presuming that they orbit further from the star; at fixed $\dot{\gamma}$, $M_{\rm comp} \propto a^2$ (Torres 1999; Liu et al. 2002).

High-resolution images can further limit the available parameter space by setting an upper limit on the semimajor axis, and a maximum brightness (and thereby mass) of any putative companions. The procedure we use to combine constraints from both radial velocities and high resolution imaging has been developed by Wright et al. (2007), Crepp et al. (2012), Montet et al. (2014), Knutson et al. (2014), Bryan et al. (2016, 2019), and others.

Speckle imaging constraints—First, we would like to convert the contrast ratios obtained through the Zorro imaging (Figure 3) to limits on the masses of putative companions and their separations from the host star.

To do this, we followed Montet et al. (2014), and opted to employ the Baraffe et al. (2003) models for substellar mass objects and the MIST isochrones for stellar mass objects (Paxton et al. 2011, 2013, 2015; Dotter 2016; Choi et al. 2016). We assumed that the system age was 5 Gyr, so that companions would have fully contracted.

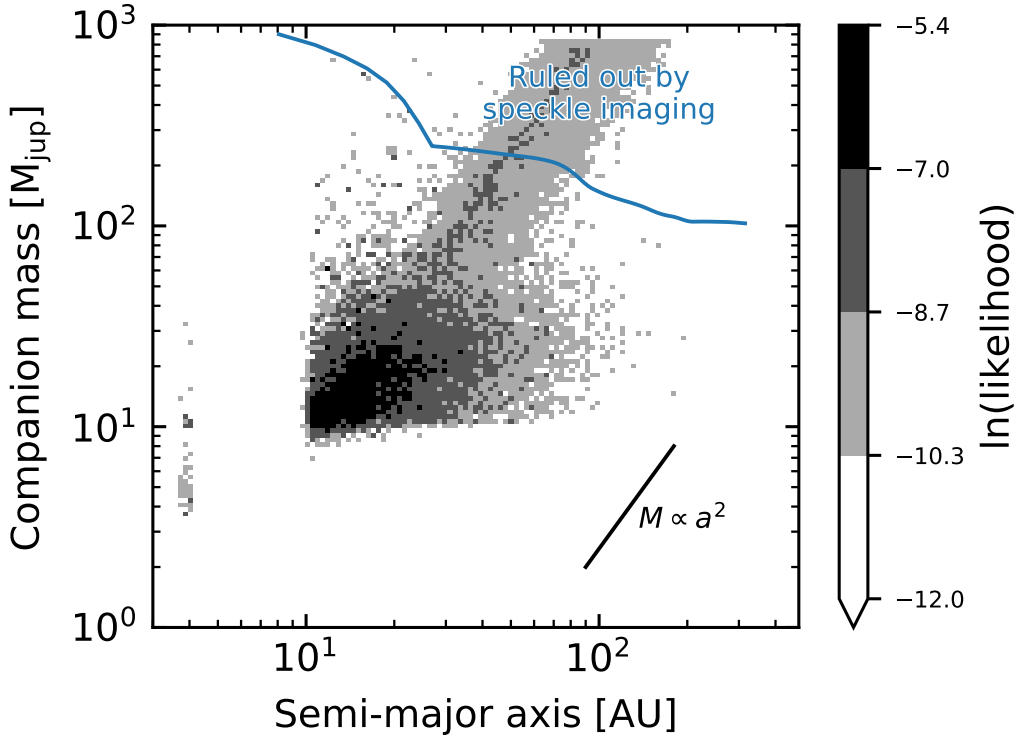

Figure 4. Masses and semi-major axes of companions that meet requirements of both the radial velocity and the speckle imaging. The likelihood inferred from radial velocities is shown in grayscale, and the region excluded from the speckle imaging is indicated (blue line). The expected mass to semimajor-axis degeneracy is shown with a black line.

Due to the custom filters of the Zorro imager, and corresponding lack of synthetic photometry, we further assumed that all sources had blackbody spectra. While this is clearly false, we do not readily have access to the planetary and stellar atmosphere models needed for the consistent calculation with the `COND03` and `MESA` models. We therefore adopted the effective temperatures and bolometric luminosities from the Baraffe et al. (2003) and MIST isochrones. Using these theoretical quantities and the empirically-measured Zorro bandpasses, we calculated absolute magnitudes in the 562 and 832 nm Zorro bands for stellar and planetary mass companions. Applying the same calculation to WASP-4 itself using the effective temperature and bolometric luminosity from B19, we derived the transformation from contrast ratio to companion mass. The resulting limits are shown in Figure 4.

Radial velocity constraints —To derive constraints on possible companion masses and separations from the radial velocities, we mostly followed the procedure of Bryan et al. (2019).

We began by defining a 128×128 grid in true planetary mass and semimajor axis, with even logarithmic spacing from 1 to $900\,M_{\rm Jup}$ and 3 to 500 AU. We then considered the possibility that an additional companion in any particular cell could explain the observed linear trend. In each cell, we simulated 512 hypothetical companions.

We assigned each companion a mass and semimajor axis from log-uniform distributions within the grid cell. We drew the inclination from a uniform distribution in $\cos i$. For companion masses less than $10\,M_{\rm Jup}$, we drew the eccentricity from Kipping (2013)'s long-period exoplanet Beta distribution ($a = 1.12$, $b = 3.09$). If the companion mass exceeded $10\,M_{\rm Jup}$, we drew the eccentricity distribution from the power-law $p_e \propto e^{\eta}$ reported by Moe & Stefano (2017) in their Equation 17. We emphasize that the long-period exoplanet and long-period binary eccentricity distributions are quite different: the exoplanet distribution is "bottom-heavy", with eccentricities preferentially close to zero. The binary star distribution is "top-heavy", with eccentricities closer to one. We chose a mass cutoff of $10\,M_{\rm Jup}$ to separate the two regimes based on the bound observed by Schlaufman (2018) between giant planets, presumably formed through core accretion, and brown dwarfs, presumably formed via gravitational instability.

For each simulated companion, we then drew a sample from the converged chains of our initial model of WASP-4b, plus its linear trend. We subtracted the planet's orbital solution, leaving RV data points with a linear trend. Given (a_c, M_c, e_c) for each simulated outer companion, and the fixed instrument offsets and jitters from the MCMC chains, we then performed a maximum likelihood fit for the time and argument of periastron of the outer simulated companion. We converted the resulting $128 \times 128 \times 512$ cube of best-fit log-likelihood values to probabilities, and averaged over the samples in each grid cell to derive a probability distribution

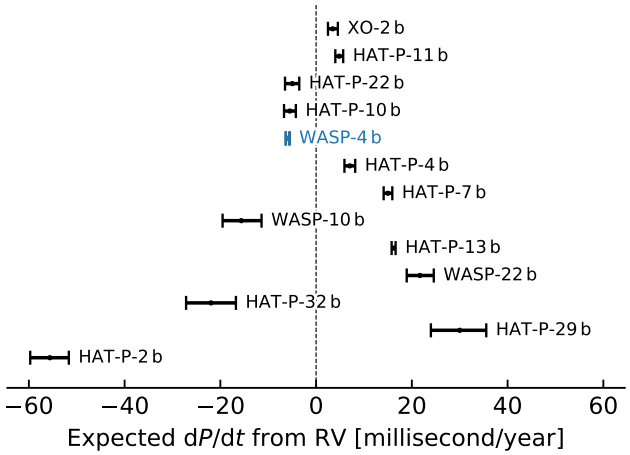

Figure 5. Predicted hot Jupiter period changes from linear radial velocity trends. Including WASP-4b, 16 of 51 hot Jupiters from Knutson et al. (2014) have shown long-term radial velocity trends. The HAT-P-11 signal is plotted, though its radial velocity signal may be caused by stellar activity. Three hot Jupiters are not plotted because their radial velocity curves better described as quadratic trends in time: HAT-P-17, WASP-8, and WASP-34. Objects are ordered in the y dimension by the absolute value of $\mathrm{d}P/\mathrm{d}t$.

in mass and semi-major axis. Figure 4 shows the result in grayscale.

4. DISCUSSION

4.1. *Implications for WASP-4*

Previous potential explanations for WASP-4b's decreasing orbital period included tidal orbital decay, orbital precession, and light-travel time effects (Bouma et al. 2019). Our new radial velocity measurements strongly indicate that the least exotic option—light-travel time effects—is also the most likely. Transits show the obital period decreasing by -8.64 ± 0.89 ms yr^{-1}; the line-of-sight acceleration observed in radial velocities would predict a period decrease of -5.94 ± 0.39 ms yr^{-1}. Though the quantitative agreement is not perfect, Occam's razor would suggest that the line of sight acceleration is probably a sufficient explanation for the apparent decrease of WASP-4b's orbital period.

The corresponding requirements for the companion causing the acceleration are that it is likely either a brown-dwarf or low mass star, and that it is between 10-100 AU from the host star (Figure 4). Given such a mass, this companion could at one time have influenced the orbital evolution of the inner giant. The fact that most hot Jupiters have similar massive outer companions (Knutson et al. 2014; Bryan et al. 2016) is circumstantial evidence for certain high-eccentricity formation channels (see Dawson & Johnson 2018). Further radial velocity monitoring should eventually reveal the orbital parameters and minimum mass of WASP-4's companion.

4.2. *How many other hot Jupiters are accelerating towards the Earth?*

We identified WASP-4b's decreasing orbital period as part of a search for tidal orbital decay. However, most hot Jupiters have companions outside of 1 AU with super-Jovian masses (Knutson et al. 2014). Line-of-sight accelerations are correspondingly relatively common in hot Jupiter systems.

To evaluate the importance of these effects in future transit timing searches, we collected the linear radial velocity trends reported by Knutson et al. (2014), and computed the expected orbital period derivatives $\dot{P}_{\mathrm{RV}} = \dot{v}_{\mathrm{r}} P / c$ for all the systems. The results are given in **Table X**, and visualized for hot Jupiters with significant linear trends in Figure 5.

Including WASP-4b, 16 of 51 hot Jupiters surveyed by Knutson et al. (2014) show a non-zero radial velocity trend. About half are positive, and half are negative. Therefore around 1 in 3 hot Jupiters are expected to show period changes commensurate with WASP-4 due to acceleration by outer companions. Half of these will be period decreases, and will be an astrophysical false positives in searches for tidal orbital decay.

4.3. *At what rate is the measurement precision of dP/dt increasing?*

For hot Jupiters that have been monitored for over baselines τ of $\approx$10 years, secular changes in their orbital periods are currently being constrained to a precision of $\lesssim 10$ ms yr^{-1} (*e.g.*, K. Patra et al. 2020, submitted). This is roughly commensurate with level of signal many outer companions are expected to induce from radial velocity accelerations (Figure 5).

It is therefore naturally of interest to ask at what point in time additional detections of the light-travel time effect can become common-place among hot Jupiters. This question is the same as asking: at what rate does the uncertainty in the quadratic term of Equation scale with the observing baseline? We take a Fisher analysis approach to the problem, following the notes by Gould (2003). Rewriting Equation 4.3 in simpler terms,

$$t_{\mathrm{tra}} = a_0 + a_1 \cdot E + a_2 \cdot E^2, \tag{7}$$

where $a_0 = t_0$, $a_1 = P$, $a_2 = 0.5 \cdot \mathrm{d}P/\mathrm{d}E$. One can then show that if N transit time measurements are taken at uniform times across a baseline of duration τ with constant precision σ_{tra}, then the uncertainty of the quadratic term is given by

$$\sigma_{a_2} = \left(\frac{25{,}920}{N} \right)^{1/2} \frac{\sigma_{\mathrm{tra}}}{\tau^4} \tag{8}$$

This result implies that if a decade passes, doubling the observing baseline, we gain a factor of 16 in precision on $\mathrm{d}P/\mathrm{d}t$. Assuming regular observations continue from ground-based telescopes (CITE) and space-based observatories (CITE TESS, CITE CHEOPS), this will enable measurements of period derivatives precise to less than 1 ms yr^{-1} before 2030.

5. CONCLUSIONS

From newly acquired radial velocity measurements, we found that WASP-4 is accelerating towards the Earth at

$\dot{\gamma} = -0.0422^{+0.0028}_{-0.0027}$ m s^{-1} yr^{-1}. The corresponding light-travel time effect predicts a period decrease $\dot{\gamma}P/c$ of -5.94 ± 0.39 ms yr^{-1}. The majority of the period decrease observed in transits ($\dot{P} = -8.64 \pm 0.89$ ms yr^{-1}) is probably explained by the acceleration of the host star — not tidal orbital decay, or apsidal precession. The companion causing the acceleration is most likely a brown dwarf or low-mass star, and its semi-major axis is likely 10-100 AU.

Over half of hot Jupiters have outer companions with masses larger than Jupiter that orbit beyond 1 AU (Knutson et al. 2014; Bryan et al. 2016). The accelerations and period changes induced by these outer companions will become an increasingly large nuisance in the hunt for orbital decay as the observational baselines get longer. In particular, the precision with which the period derivative can be measured scales as the fourth power of the baseline duration (§ 4.3), and so within a decade many more hot Jupiters should show orbital period changes due to accelerations induced by their outer companions. This effect can be distinguished from tidal orbital decay through long-term radial velocity monitoring of hot Jupiters.

Software: `astrobase` (Bhatti et al. 2018), `astroplan` (Morris et al. 2018), `astropy` (Collaboration et al. 2018), `astroquery` (Ginsburg et al. 2018), `corner` (Foreman-Mackey 2016), `emcee` (Foreman-Mackey et al. 2013), `IPython` (Pérez & Granger 2007), `matplotlib` (Hunter 2007), `MESA` (Paxton et al. 2011, 2013, 2015) `numpy` (Walt et al. 2011), `pandas` (McKinney 2010), `radvel` (Fulton et al. 2018), `scipy` (Jones et al. 2001).

Table 1. Best-fit transit timing model parameters.

Parameter	Median Value (Unc.)[a]
Constant period	
t_0 [BJD$_{\rm TBD}$]	2455804.515752(+19)(-19)
P [days]	1.338231466(+23)(-22)
Constant period derivative	
t_0 [BJD$_{\rm TBD}$]	2455804.515918(+24)(-24)
P [days]	1.338231679(+31)(-31)
dP/dt	$-4.00(+37)(-38) \times 10^{-10}$

[a] **FIXME table needs numbers** The numbers in parenthesis give the 68% confidence interval for the final two digits, where appropriate.

REFERENCES

Baluev, R. V., Sokov, E. N., Jones, H. R. A., et al. 2019, arXiv:1908.04505 [astro-ph], arXiv: 1908.04505

Baraffe, I., Chabrier, G., Barman, T. S., Allard, F., & Hauschildt, P. H. 2003, A&A, 402, 701

Beerer, I. M., Knutson, H. A., Burrows, A., et al. 2011, ApJ, 727, 23

Bhatti, W., Bouma, L. G., & Wallace, J. 2018, `astrobase`

Bonomo, A. S., Desidera, S., Benatti, S., et al. 2017, A&A, 602, A107

Bouma, L. G., Winn, J. N., Baxter, C., et al. 2019, AJ, 157, 217

Bryan, M. L., Knutson, H. A., Lee, E. J., et al. 2019, AJ, 157, 52

Bryan, M. L., Knutson, H. A., Howard, A. W., et al. 2016, ApJ, 821, 89

Choi, J., Dotter, A., Conroy, C., et al. 2016, ApJ, 823, 102, arXiv: 1604.08592

Collaboration, T. A., Price-Whelan, A. M., Sipöcz, B. M., et al. 2018, arXiv:1801.02634 [astro-ph], arXiv: 1801.02634

Crepp, J. R., Johnson, J. A., Howard, A. W., et al. 2012, ApJ, 761, 39

Dawson, R. I., & Johnson, J. A. 2018, Annual Review of Astronomy and Astrophysics, 56, 175

Dotter, A. 2016, ApJS, 222, 8

Feng, Y. K., Wright, J. T., Nelson, B., et al. 2015, The Astrophysical Journal, 800, 22

Foreman-Mackey, D. 2016, The Journal of Open Source Software, 24

Foreman-Mackey, D., Hogg, D. W., Lang, D., & Goodman, J. 2013, PASP, 125, 306

Fulton, B. J., Petigura, E. A., Blunt, S., & Sinukoff, E. 2018, arXiv:1801.01947 [astro-ph], arXiv: 1801.01947

Giménez, A., & Bastero, M. 1995, Ap&SS, 226, 99

Ginsburg, A., Sipocz, B., Madhura Parikh, et al. 2018, Astropy/Astroquery: V0.3.7 Release

Goodman, J., & Weare, J. 2010, Communications in Applied Mathematics and Computational Science, 5, 65

Gould, A. 2003, arXiv Astrophysics e-prints, arXiv:astro

Howard, A. W., Johnson, J. A., Marcy, G. W., et al. 2010, ApJ, 721, 1467

Hunter, J. D. 2007, Computing in Science & Engineering, 9, 90

Husnoo, N., Pont, F., Mazeh, T., et al. 2012, MNRAS, 422, 3151

Jones, E., Oliphant, T., Peterson, P., et al. 2001, Open source scientific tools for Python

Kass, R. E., & Raftery, A. E. 1995, Journal of the American Statistical Association, 90, 773

Kipping, D. M. 2013, MNRAS:l, 434, L51

Knutson, H. A., Fulton, B. J., Montet, B. T., et al. 2014, ApJ, 785, 126

Levrard, B., Winisdoerffer, C., & Chabrier, G. 2009, ApJ, 692, L9

Liu, M. C., Fischer, D. A., Graham, J. R., et al. 2002, The Astrophysical Journal, 571, 519

Matsumura, S., Peale, S. J., & Rasio, F. A. 2010, ApJ, 725, 1995

McKinney, W. 2010, in Proceedings of the 9th Python in Science Conference, ed. S. van der Walt & J. Millman, 51

Moe, M., & Stefano, R. D. 2017, The Astrophysical Journal Supplement Series, 230, 15

Montet, B. T., Crepp, J. R., Johnson, J. A., Howard, A. W., & Marcy, G. W. 2014, ApJ, 781, 28

Morris, B. M., Tollerud, E., Sipőcz, B., et al. 2018, AJ, 155, 128

Patra, K. C., Winn, J. N., Holman, M. J., et al. 2017, AJ, 154, 4

Paxton, B., Bildsten, L., Dotter, A., et al. 2011, ApJS, 192, 3

Paxton, B., Cantiello, M., Arras, P., et al. 2013, ApJS, 208, 4

Paxton, B., Marchant, P., Schwab, J., et al. 2015, ApJS, 220, 15

Pérez, F., & Granger, B. E. 2007, Computing in Science and Engineering, 9, 21

Petrucci, R., Jofré, E., Schwartz, M., et al. 2013, ApJL, 779, L23

Pont, F., Husnoo, N., Mazeh, T., & Fabrycky, D. 2011, MNRAS, 414, 1278

Rasio, F. A., Tout, C. A., Lubow, S. H., & Livio, M. 1996, The Astrophysical Journal, 470, 1187

Schlaufman, K. C. 2018, arXiv:1801.06185 [astro-ph], arXiv: 1801.06185

Scott, N. J., Howell, S. B., Horch, E. P., & Everett, M. E. 2018, PASP, 130, 054502

Southworth, J., Dominik, M., Jorgensen, U. G., et al. 2019, arXiv:1907.08269 [astro-ph], arXiv: 1907.08269

Torres, G. 1999, Publications of the Astronomical Society of the Pacific, 111, 169

Triaud, A. H. M. J., Collier Cameron, A., Queloz, D., et al. 2010, A&A, 524, A25

Vogt, S. S., Allen, S. L., Bigelow, B. C., et al. 1994, SPIE Conference Series, Vol. 2198, SPIE Conference Series, ed. D. L. Crawford & E. R. Craine, 362

Walt, S. v. d., Colbert, S. C., & Varoquaux, G. 2011, Computing in Science & Engineering, 13, 22

Wilson, D. M., Gillon, M., Hellier, C., et al. 2008, ApJL, 675, L113

Wright, J. T., Marcy, G. W., Butler, R. P., & Vogt, S. S. 2004, ApJS, 152, 261

Wright, J. T., Marcy, G. W., Fischer, D. A., et al. 2007, ApJ, 657, 533

Yee, S. W., Winn, J. N., Knutson, H. A., et al. 2020, The Astrophysical Journal Letters, 888, L5